ELSEVIER

International Journal of Mass Spectrometry 195/196 (2000) 285–302

International Journal of Mass Spectrometry

Internal energy distributions resulting from sustained off-resonance excitation in FTMS. I. Fragmentation of the bromobenzene radical cation

Julia Laskin[1], Michelle Byrd, Jean Futrell[1,*]

Department of Chemistry and Biochemistry, University of Delaware, Newark, DE 19716, USA

Received 3 June 1999; accepted 24 August 1999

Abstract

Collision energy resolved study of the fragmentation of $C_6H_5Br^+$ was carried out using both on-resonance and sustained off-resonance excitation. Fragmentation efficiency curves were obtained as a function of collision energy under single- and multiple-collision conditions. The results were modeled using the Rice–Ramsperger–Kassel–Marcus/quasi-equilibrium theory (RRKM/QET) formalism. An analytical form for the collisional energy deposition function is proposed. Experimental results obtained in both on-resonance single-collision and sustained off-resonance irradiation (SORI) experiments could be reproduced within the same theoretical model. The influence of the center-of-mass collision energy and pressure on energy transfer is demonstrated. (Int J Mass Spectrom 195/196 (2000) 285–302) © 2000 Elsevier Science B.V.

Keywords: SORI-CID; Multiple collisions; Energy deposition function; Bromobenzene

1. Introduction

Collision-induced dissociation (CID) is a powerful tool both for determination of ion structures in the gas phase and for obtaining information on energetics and mechanisms of fragmentation processes of internally excited ions. Various aspects of collisional activation of polyatomic ions have been extensively reviewed [1–4]. High-energy processes, involving collision energies in the keV range, are commonly carried out on sector instruments, whereas low-energy CID measurements (<100 eV) are commonly implemented using triple quadrupole instruments or ion traps [Fourier transform ion cyclotron resonance (FTICR), quadrupole ion trap, etc.]. With increasing complexity of the ion of interest it becomes increasingly difficult to induce dissociation using traditional collision activation (CA) methods, i.e. ion activation under single collision conditions. This difficulty arises from two principal factors: (1) Rates of decomposition decrease dramatically with an increase in the number of internal degrees of freedom (see [4] for an extensive discussion). Consequently, very high internal energy has to be deposited into the ion in order to induce fragmentation on the mass spectrometer timescale,

* Corresponding author.

[1] Present address: Pacific Northwest National Laboratory, William R. Wiley Environmental Molecular Sciences Laboratory, P.O. Box 999 (K8-84), Richland, WA 99352.

Dedicated to Bob Squires for his many seminal contributions to mass spectrometry and ion chemistry.

PII S1387-3806(99)00185-2

which ranges from microseconds for sector instruments to seconds for ion traps. (2) Center-of-mass (CM) collision energy and, consequently, the maximum energy available for CA decreases with an increase in ion mass (m_{ion}) in the ratio $m_n/(m_{ion} + m_n)$, where m_n is the neutral target mass. As discussed elsewhere [2] the actual energy deposited upon collision between the ion and neutral target is much less than the CM maximum value.

In order to overcome these difficulties, various "slow heating" methods have been developed to study fragmentation of large molecules, e.g. peptides and proteins [5]. These techniques include infrared multiphoton dissociation (IRMPD) [5–8], blackbody infrared dissociation [9–12], and low-energy collisional activation employing multiple collisions [13–15]. Sustained off-resonance irradiation (SORI) is one of the commonly used "slow heating" methods in Fourier transform ion cyclotron resonance mass spectrometry (FTICR) [13,16]. In this method a radiofrequency excitation pulse is applied slightly off the resonant frequency of the ion being investigated, causing the ion's kinetic energy to oscillate with time. During excitation the ion is activated by collisions with neutral atoms or molecules. To ensure multiple-collision conditions, the ion is excited for hundreds of milliseconds. As the ion collides with the target gas, its internal energy slowly increases and the ion fragments when sufficient energy transfer from translation to internal energy has occurred. Marzluff and Beauchamp [5] demonstrated that the activation process by such low-energy collisions of the ion with neutral gas becomes more efficient as the size of the ion increases. The increased efficiency in energy transfer is attributed to multiple interactions of the target molecule with different atoms in the ion during a single collision event.

Collision-induced dissociation of polyatomic ions generally proceeds via a two-step process of collisional activation followed by subsequent unimolecular dissociation of the internally excited ion. The rate of unimolecular fragmentation depends on the internal energy content of the ions. It is well known that these collisionally activated ions have a wide distribution of internal energies (E). This distribution for a particular CM energy (E_{CM}) is described by the collisional energy deposition function (CEDF). Once the CEDF is known, the energetics and dynamics of unimolecular fragmentation as a function of collisional activation parameters can be placed on a quantitative basis. In the discussion that follows, $P(E, E_{CM})$ denotes the energy deposition function.

A number of studies have been performed to determine $P(E, E_{CM})$ from experimental CID spectra. The dynamics of low-energy CID of benzene ions have been investigated using a crossed-beam instrument [17] over a range of collision energies and scattering angles. The overall CEDF was deduced by integrating the measured velocity- and angular-resolved contours for all fragment ions, establishing a most probable energy transfer of about 6 eV at a 17 eV CM energy. In this direct measurement of the CEDF a relatively broad distribution of energy deposition was found. Although energy- and angle-resolved studies provide a direct experimental determination of CEDF, these experiments are difficult to perform and, consequently, have been carried out thus far for only relatively small molecules. Alternatively, several indirect methods for determining CEDF have been proposed. A probability theory-based method has been developed by Kim [18] for high-energy tandem mass spectrometry CID to account for the effects of sequential collisional excitation in a small number of collisions. Analysis of pressure dependence of the CID of a methane molecular ion based on this theory led to an analytical expression for the CEDF for high-energy collisions [19]. A different approach has been used by Cooks and co-workers [20] for a system of consecutive reactions with known endothermicities and similar entropy requirements. The relative abundance of each fragment ion is taken as a measure of the number of ions produced with internal energies lying in the energy range where that particular fragment ion is dominant. Only a relatively crude estimate for the CEDF may be obtained using this approach.

It has been demonstrated that collision energy resolved mass spectrometric studies (CERMS) using a FTICR mass spectrometer can be used to deduce thermochemical information [21–23]. In these experiments ions are accelerated to the desired kinetic

energy by an on-resonance rf pulse of known amplitude and duration. The advantage of this excitation method over SORI-CID is that the kinetic energy of ions is well defined, making the on-resonance CID a valid method for threshold measurements. The main difficulty in using FTICR for threshold measurements is the limited dynamic range. Relative signal intensities may be accurately measured only over three orders of magnitude compared to six orders of magnitude readily achieved using sector or triple quadrupole instruments [24]. The dynamic range problem makes this type of experiment quite tedious to perform under single-collision conditions. To eliminate multiple-collision excitation, the relative intensity of fragment ions detected under single-collision conditions must be maintained below 2% (see for example [23]). SORI-CID is an alternative method that enhances the extent of fragmentation using multiple collisions and long activation times. However, off-resonance excitation results in ill-defined kinetic energy of the ions and shifts appearance energies of fragment ions to low values. For this reason very little information on the energetics and dynamics of fragmentation has been obtained using SORI-CID.

To date SORI-CID studies typically report dissociation mechanisms rather than energy transfer in the activation step. To the best of our knowledge, the first attempt to characterize the energy transfer upon SORI-CID quantitatively is a study of fragmentation of $Cr(CO)_6^+$ carried out in our group [25]. Very recently Williams and co-workers have determined "effective temperatures" of protonated leucine enkephalin and doubly protonated bradykinin by comparing the dissociation kinetics following SORI-CID to that obtained under blackbody infrared dissociation (BIRD) conditions [26]. They found that the effective temperatures of both peptides dissociated under the same SORI-CID conditions are similar. The influence of different experimental parameters on the effective temperature was investigated.

The present study is the first step in characterizing the energy deposition function upon SORI-CID using the collision energy-resolved fragmentation of the bromobenzene radical cation as a model [27]. Fragmentation efficiency curves as a function of collision energy were obtained under single and multiple-collision conditions for CM collision energies up to 20 eV. These data were analyzed to determine both the amount of energy deposited into the ion and the change in the internal energy distribution as a function of collision energy and number of collisions. We propose an analytical form for the CEDF based on these experiments.

The lowest energy fragmentation pathway of the bromobenzene radical cation $C_6H_5Br^{\cdot +}$ involves a simple C–Br bond cleavage yielding phenyl cation $C_6H_5^+$ and bromine atom (R1).

$$C_6H_5Br^{\cdot +} \rightarrow C_6H_5^+ + Br^{\cdot} \quad \text{(R1)}$$

Unimolecular fragmentation of the bromobenzene radical cation has been studied by various techniques [28–33] and the energetics of Reaction (R1) is well established. CID of $C_6H_5Br^+$ with N_2 as a neutral target has been studied previously by Douglas in a triple quadrupole mass spectrometer [34] and very high efficiency of energy transfer was established. For example, at a CM collision energy of 8 eV more than 40% of the translational energy is transferred to internal energy in essentially every collision. For these reasons we chose bromobenzene as a model to define energy transfer during multiple-collision SORI-CID.

2. Experimental

2.1. General

Experiments were performed on the University of Delaware 7T Bruker BioApex FTICR Mass Spectrometer equipped with an Infinity Cell. The system is operated at an indicated base pressure of 5×10^{-10} Torr. Ions were generated in an external electron impact (EI) ionization source. Low electron energy (11–13 eV) was used to suppress the extent of electronic and vibrational excitation of $C_6H_5Br^{\cdot +}$ (*m/z* 156) in the ion source. Ions were transferred into the ICR cell by a series of ion transfer lenses and captured in the cell using the Sidekick mechanism for ion accumulation. Ions were trapped in the cell by apply-

ing a 2 V potential to the trapping plates. Excess kinetic energy was removed from the ions by pulsing Ar into the cell for a duration of about 300 ms at a maximum pressure of 2×10^{-6} Torr (see Sec. 2.2 for details of pressure calibration). Ions were allowed to cool to thermal equilibrium by radiative and collisional cooling during the pumping delay of 5–10 s. Changing the cooling delay time from 5–60 s has no effect on the appearance of CID spectra of bromobenzene, thus confirming that the ions were thermalized prior to collisional activation. Undesired ions were ejected from the cell using a correlated sweep procedure. A second Ar pulse was then introduced to remove any excess kinetic energy gained by the molecular ions during the isolation event. When necessary, a correlated-shots method was used to eject any remaining fragment ions at *m/z* 77.

For SORI-CID experiments a third Ar pulse was introduced into the cell for collisional activation. Ions of *m/z* 156 were radially excited slightly off resonance ($\Delta f = -700$ Hz) for 100 ms at nearly fixed Ar pressure (see Sec. 2.3 for details). For the 100-collision experiment, sequential Ar pulses were used to maintain nearly constant gas pressure during 1-s SORI excitation. The kinetic energy of the ions was incremented by changing the peak-to-peak voltage applied to the excitation plates. The ratio between the peak-to-peak voltage measured directly on the excitation plates and on the output leads from the rf amplifier was determined prior to the series of experiments reported here. The output voltage of the amplifier was monitored during each experiment and the calibrated ratio was used to calculate the amplitude of the excitation rf signal. After a 5 s pumping delay the cell ions were excited for detection by broadband chirp excitation.

For on-resonance CID experiments a static Ar pressure ($2–4 \times 10^{-8}$ Torr) was maintained in the ICR cell. Ions were radially excited to a predefined radius by an on-resonance rf pulse of constant peak-to-peak voltage (10 V). The kinetic energy of the ions was varied by changing the duration of the rf pulse between 100 and 300 μs. Ions were allowed to undergo collisions with Ar during a 50 ms delay time (t_{CID}). After the CID delay ICR excitation and detection were carried out with a relatively short (5 ms) acquisition time relative to the time of CID event. We verified that no detectable fragmentation occurred during the acquisition time. Finally, a quench pulse was used to remove all ions from the cell.

Each mass spectrum used in the data analysis was an average of 10 scans. From the set of spectra at different collision energies, a plot of the relative precursor and fragment ion abundance as a function of the center-of-mass energy of the precursor ion was constructed. In the present study these curves are referred to as fragmentation efficiency curves.

2.2. Ion energetics

The kinetic energy of the ions in the laboratory frame is given by Eq. (1) [35]

$$E_{\text{lab}} = \frac{q^2 E_0^2}{4m(\omega - \omega_c)^2}[1 - \cos(\omega - \omega_c)t] \tag{1}$$

where m and q are the mass and the charge of the ion, respectively; ω_c is the cyclotron frequency of the ion; ω is the frequency of the excitation field; and E_0 is the amplitude of the electric field. The latter term may be expressed in terms of peak-to-peak excitation voltage ($V_{\text{p–p}}$), the geometry factor of the infinity cell ($\beta = 0.9$), and the diameter of the cell (d) as given by Eq. (2) [36]

$$E_0 = \frac{\beta V_{\text{p–p}}}{2d} \tag{2}$$

Substituting this equation for E_0 gives Eq. (3):

$$E_{\text{lab}} = \frac{\beta^2 q^2 V_{\text{p–p}}^2}{16md^2\Delta\omega^2}[1 - \cos(\omega - \omega_c)t] \tag{3}$$

The maximum kinetic energy (peak-to-peak) achieved by off-resonance CID is given by:

$$E_{\text{lab}} = \frac{\beta^2 q^2 V_{\text{p–p}}^2}{8md^2\Delta\omega^2} \tag{4}$$

For the limiting case where $\Delta\omega = 0$, which is the case for on-resonance CID, the expression $[1 - \cos(\omega - \omega_c)t]/\Delta\omega^2$ collapses to 1/2, and the maximum kinetic energy of the ion is

$$E_{lab} = \frac{\beta^2 q^2 V_{p-p}^2 t^2}{32md^2} \quad (5)$$

where t is the excitation time. The same expression for the on-resonance excitation has been used by Sievers et al. [23]. It should be noted that Eq. (5) differs by a factor of 1/2 from the one proposed by Grosshans and Marshall [37]. This factor accounts for the two counter-rotating components of the linearly polarized electric field (see [23] for discussion). Finally the center-of-mass collision energy E_{CM} was calculated from E_{lab} using the following expression:

$$E_{CM} = \frac{M}{M + m} E_{lab} \quad (6)$$

where M is the mass of the neutral molecule.

2.3. Pressure calibration

Accurate pressure calibration is required in order to perform CID experiments under well-defined conditions. The pressure in the cell is monitored using a cold cathode gauge located close to the cryopump and approximately one meter from the ICR cell. Because the vacuum chamber is actively pumped the pressure reading on the gauge is significantly lower than the actual pressure in the cell. The factor between the pressure reading and the pressure in the cell was determined from the rate measurement for the electron transfer reaction between vibrationally excited N_2^+ and Ar

$$Ar + N_2^+(v = 1) \rightarrow Ar^+ + N_2$$

The rate constant reported in the literature [38] for this reaction is 4×10^{-10} cm^3/s. The reaction of N_2^+ ($v = 0$) with Ar is slightly endothermic, and its rate constant is more than two orders of magnitude lower than the above reaction.

N_2^+ was produced in an external electron impact ion source using low-energy electrons (20 eV) and transferred into the cell. Static Ar pressure (5×10^{-9}–5×10^{-8} Torr according to cold cathode gauge reading) was maintained in the cell. The decrease in N_2^+ signal was monitored as a function of time. Assuming pseudo-first-order reaction with respect to [Ar], the pressure of the neutral target was determined from the slope of ln[N_2^+] versus time and the reported rate constant. The slow reaction component was dominant only at long times. For example, at 1×10^{-8} Torr no measurable contribution from the slow reaction was observed during the first 0.5 s. This contribution was ignored because by that time the fast reaction was already completed. We have also checked that the same rate constant was obtained from a two-exponential fit of the entire curve of [N_2^+] versus time measured up to 5 s. Rate measurements were performed at different static Ar pressures and the factor between the pressure reading and the actual pressure in the cell was derived. The factor 1.55 ± 0.25 is an average value determined from these measurements.

For the SORI-CID experiments discussed in this article, Ar was introduced into the ICR cell using a pulse valve. Thus the pressure in the cell varied with time. The time-dependent pressure of Ar in the cell was monitored using a time-domain damping method. There are two principal mechanisms for signal damping in FTICR [39]—namely inhomogeneous damping resulting from inhomogeneities in the electric or magnetic field and homogeneous relaxation resulting mainly from collisions between ions and a neutral target. It has been shown that for exponential collisional damping, the relaxation time (τ) is inversely proportional to the gas pressure in the cell, P [40]. In order to obtain a relationship between P and τ we first constructed a calibration curve (damping time versus pressure) by measuring relaxation times at different static Ar pressures in the cell (2×10^{-9}–5×10^{-6} Torr pressure reading on the cold cathode gauge).

Molecular ions generated in an external source were transferred into the cell and then radially accelerated by “chirp” excitation (m/z range, 150–250 u). Because we are interested solely in collisional damping of the signal, the potentials applied to the Sidekick assembly and the trapping plates were adjusted to minimize inhomogeneous damping under high vacuum conditions. Homogeneous (collisional) damping is the dominant process under all conditions of interest here. Detection times longer than three relaxation

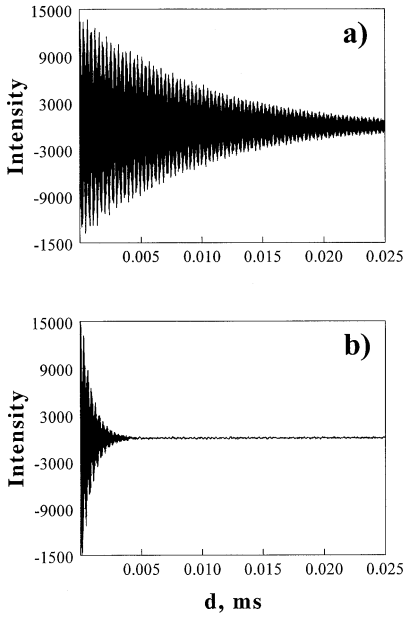

Fig. 1. Damped time-domain (transient) signals for static Ar pressures of (a) 1×10^{-7} and (b) 1×10^{-6} Torr.

times were chosen in order to sample a sufficient part of the exponential. Fig. 1(a) and (b) show typical transient signals for Ar pressures of 1×10^{-7} and 1×10^{-6} Torr. As expected, the signal damps much faster at higher pressure. Relaxation times for different static Ar pressures were extracted from the corresponding time-domain signals. The correlation between relaxation time and pressure in the cell is shown in Fig. 2.

The experimental sequence for dynamic pressure calibration is presented in Fig. 3. The timescale was

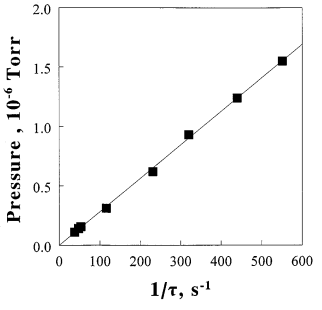

Fig. 2. Correlation between relaxation time and the pressure in the cell.

determined by varying the delay between opening of the pulse valve and the detection event. A short detection time (5–10 ms) was used to sample most of the profile. However, longer detection times (up to 50 ms) were used to measure the tail of the profile for which longer damping times were sampled. Ar pressure versus delay time between the pulse valve opening and detection event (d) was obtained with backing pressure of 3.3 Torr and valve open times of 5 and 50 ms [see Fig. 4 (a, b)]. The profiles show a peak in pressure at ~100–120 ms with full width at half maximum (FWHM) of about 170 ms.

Relaxation times at a delay of 100 ms (at the maximum of the profile) were measured with different open times of the valve (Δ) and different backing pressures. Actual pressure in the cell was derived from measured relaxation time using the correlation shown in Fig. 2. Typical results (backing pressure 3.3 Torr) obtained from these experiments are presented in Fig. 5. These results were used to control pressure conditions in subsequent SORI-CID experiments.

2.4. Distribution of the number of collisions

Knowledge of the number of collisions is of crucial importance in obtaining accurate CID data. Great care must be taken to ensure single-collision conditions in order to obtain meaningful bond dissociation energies from experimental CID thresholds (see, for example, [21]). We will show in Sec. 3.2 that, for multiple collision experiments, the average number of collisions is an important experimental parameter that strongly influences the extent of fragmentation.

The probability (Q_n) that the ion encounters n atoms during the CID delay may be approximated by the Poisson distribution [18]:

$$Q_n = \frac{e^{-a}a^n}{n!} \tag{7}$$

where $a = \nu t_{\mathrm{CID}}$ is the average number of collisions during the CID delay t_{CID} for a collision frequency ν. Fig. 6(a) and (b) compare distributions of the number of collisions calculated for $a = 0.02$ and $a = 1$ [Fig. 6(a)], $a = 1$ and $a = 10$ [Fig. 6(b)]. In the case

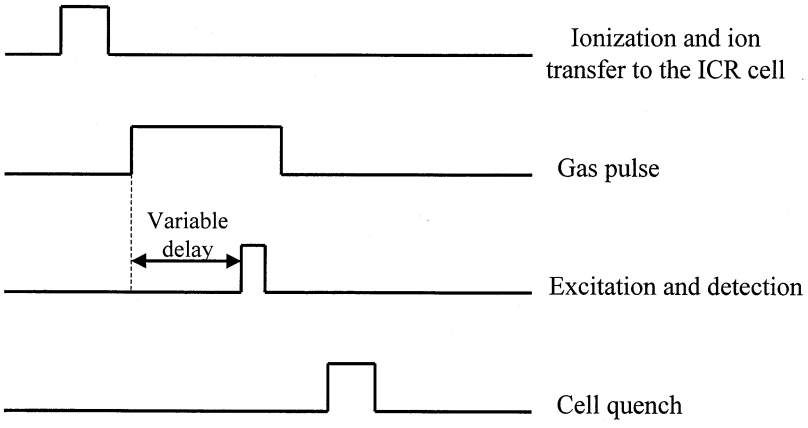

Fig. 3. The experiment sequence for dynamic pressure calibration.

where the average collision number equals one, the fraction of ions that undergo one collision is ~36% [Fig. 6(a)]. Note that a significant number of ions undergo more than one collision during the CID delay (the ratio of double to single collisions Q_2/Q_1 is 0.5 in this case). In order to ensure that the observed fragmentation results entirely from single-collision activation, the collision frequency must be reduced by more than an order of magnitude [see Fig. 6(a), $a = 0.02$]. The ratio of single to double collisions Q_2/Q_1 is only 0.01 for $a = 0.02$, meaning that the contribution of double collisions to the observed fragmentation is negligible.

For multiple-collision CID experiments the requirements are less rigorous. The distribution of the number of collisions for multiple-collision conditions has a shape similar to a Gaussian function [Fig. 6(b)]. For the 10-collision experiment illustrated, the

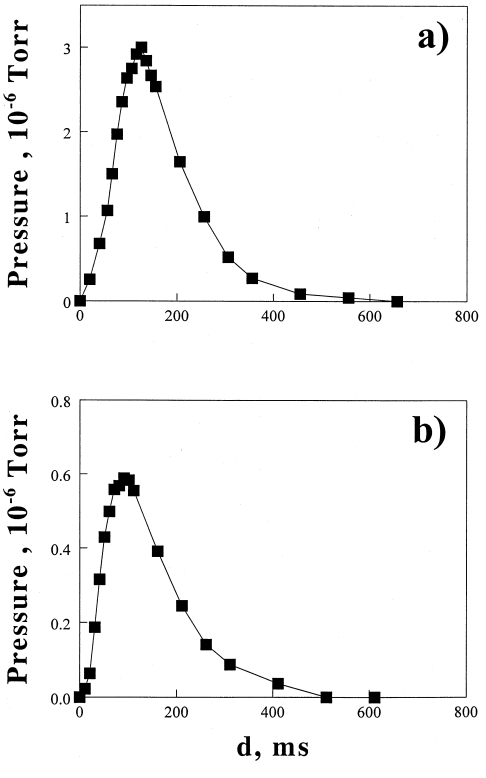

Fig. 4. Pressure profiles obtained with backing pressure of 3.3 Torr and (a) 50 ms and (b) 5 ms valve open times. *d* is the delay between pulse valve opening and the detection event.

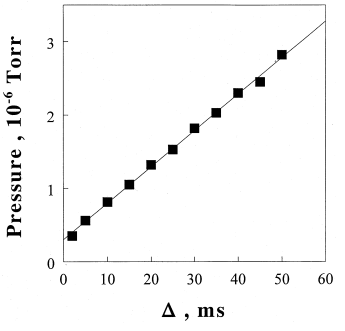

Fig. 5. Gas pressure measured at the maximum of the pressure profile as a function of different open times of the pulse valve (Δ).

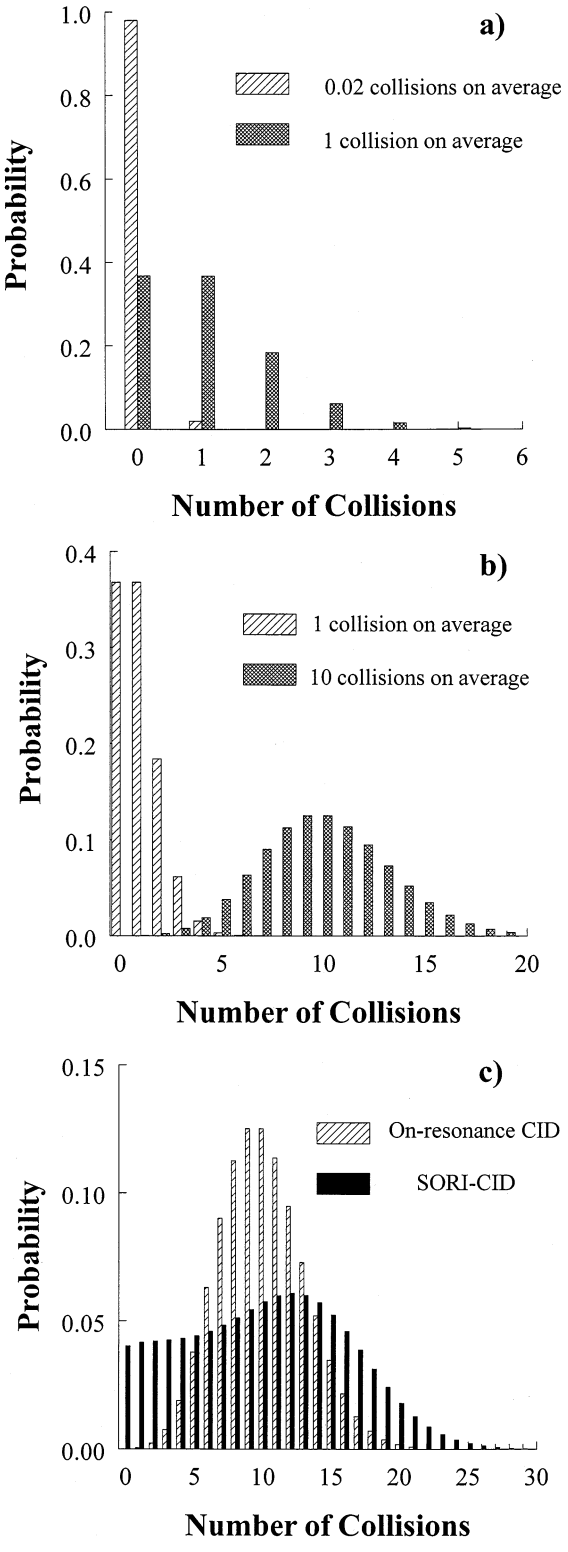

FWHM of the distribution is seven; i.e. a significant percentage of the ions undergo less than 10 collisions or more than 10 collisions during the time of ion activation (t_{CID}). It is important to note that the distributions, shown in Fig. 6(a) and (b), were obtained without taking into account collisional damping of the ion kinetic energy. The damping is important for the on-resonance experiment and leads to the exponential (or close to exponential) decay in the kinetic energy of the ions as a result of collisions with the neutral target. Although we assumed that Q_n does not depend on time for the on-resonance excitation, it is definitely time dependent, primarily because of collisional damping.

It was previously mentioned that the kinetic energy and, consequently, the velocity of the ions during SORI excitation oscillate with time. For the constant cross section (hard sphere collisions) the collision frequency is the product of cross section times velocity. Hence the collision frequency is a function of the square root of kinetic energy of the ion (this contrasts to very low energy collisions for which Langevin theory cross sections are inversely dependent on velocity and the collision frequency is constant). For this reason Q_n is also time dependent. The distribution of the number of collisions for SORI-CID experiments may be obtained by averaging Q_n [Eq. (7)] over time. This yields an average probability, $\langle Q_n \rangle$, for an ion to undergo n collisions during t_{CID}. The distribution of $\langle Q_n \rangle$ giving 10 collisions on average, together with the corresponding distribution for the on-resonance experiment, is shown in Fig. 6(c). Because the collision frequency for low energy ions is much lower than the collision frequency for energetic ions, the distribution for the SORI excitation is asymmetric with much higher weight for small values of n. As a result, the average number of collisions obtained from the distribution is lower than the collision frequency,

Fig. 6. Distributions of the number of collisions for (a) $a = 0.02$ and $a = 1$; (b) $a = 1$ and $a = 10$; (c) the distribution for SORI-CID averaged over excitation time, $\langle Q_n \rangle$, giving rise to 10 collisions on average and the corresponding distribution based on Eq. (7) for $a = 10$.

Table 1
Correlation between collision number (a) and the average number of collisions (N_{av}) for SORI-CID

a	3	5	10	15	20	100
N_{av}	1.9	3.2	6.3	9.5	12.6	63

a, used to simulate the distribution. Table 1 summarizes the correlation between the average number of collisions and collision frequency over the range of interest in SORI experiments.

3. Results and discussion

3.1. On-resonance CID

Bromine atom loss from the bromobenzene radical cation is the only fragmentation channel observed using on-resonance CID under single-collision conditions. The fragmentation efficiency curve for the formation of $C_6H_5^+$ (*m/z* 77) is shown in Fig. 7. A theoretical threshold function that takes into account Doppler broadening, developed by Chantry [41], was employed in this study to extract the appearance energy (AE) for Reaction (R1) from the experimental data. The value 2.6 ± 0.2 eV at 298 K was obtained from the best fits of the threshold region of the

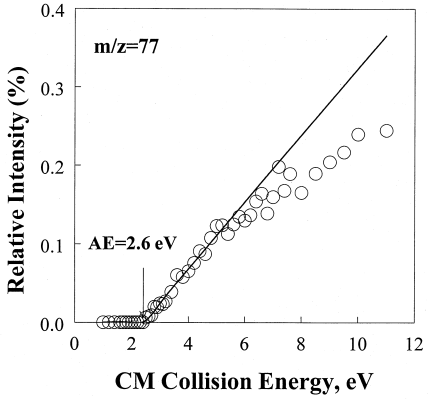

Fig. 7. Fragmentation efficiency curve for $C_6H_5^+$ formation for on-resonance CID of the bromobenzene radical cation under single-collision conditions (open circles) and theoretical threshold function (line) developed by Chantry [41].

experimental fragmentation efficiency curves. This leads to the appearance energy of 2.7 ± 0.2 eV at 0 K when corrected for the average thermal energy of bromobenzene at 298 K. This result is in excellent agreement with the 0 K threshold values obtained by Dunbar and Honovich [31], E_0 = 2.81 ± 0.07 eV and by both Rosenstock et al. [33] and Malinovich et al. [30], E_0 = 2.76 ± 0.05 eV.

3.2. SORI-CID at different pressures

SORI-CID measurements were performed at different pressures of the neutral target. The pressure was carefully controlled to ensure a constant collision frequency over a range of CM energies. SORI excitation was performed during the time when the Ar pressure in the cell was almost constant and close to the maximum [see Fig. 4(a) and (b)]. Experimental results were obtained under conditions giving rise to collision number a = 3, 5, 10, 15, 20, and 100 during SORI excitation.

Fig. 8(a) and (b) show typical sets of fragmentation efficiency curves obtained using SORI excitation of bromobenzene for a = 3 and 20. As expected, fragmentation yields for all fragment ions are significantly higher at higher pressure. Similar to the single-collision experiment, $C_6H_5^+$ (*m/z* 77) is the only fragment observed at low center-of-mass energies (energy range from 1.5–5 eV). The ion $C_4H_3^+$ (*m/z* 51), formed by C_2H_2 loss from $C_6H_5^+$, is observed at collision energies above 5 eV. At energies higher than 11 eV, the ion of *m/z* 50 ($C_4H_2^{\cdot+}$) is also formed. This fragment can be produced either directly from $C_6H_5^+$ or from secondary decomposition of $C_4H_3^+$.

Vanishing current values of appearance energies for the formation of $C_6H_5^+$, $C_4H_3^+$, and $C_4H_2^{\cdot+}$ were derived from the fragmentation efficiency curves. The average appearance energy 1.6 ± 0.2 eV for $C_6H_5^+$ (*m/z* 77) formation determined from our measurements was found to be pressure independent. This value is much lower than 2.6 ± 0.2 eV, derived from the on-resonance single-collision experiment. This is not surprising because multiple collisions between an ion and neutral target cause experimental appearance energies to shift toward lower values. It is interesting

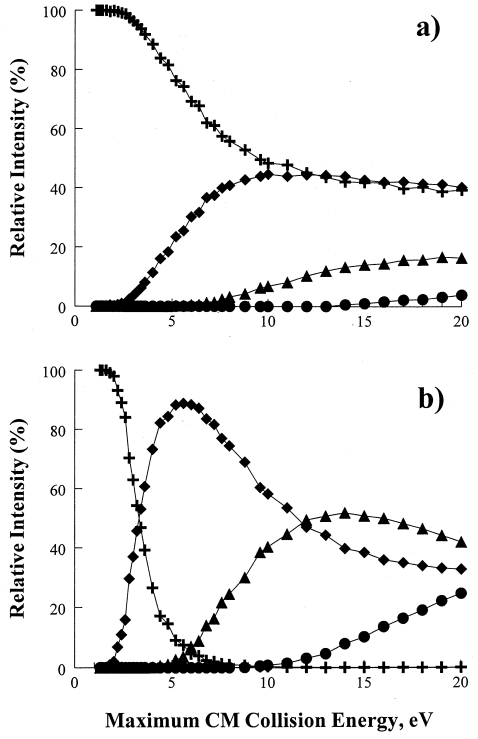

Fig. 8. Typical sets of fragmentation efficiency curves obtained using SORI excitation for collision number (a) $a = 3$ and (b) $a = 20$. (cross) *m/z* 156; (diamond) *m/z* 77; (triangle) *m/z* 51; (circle) *m/z* 50.

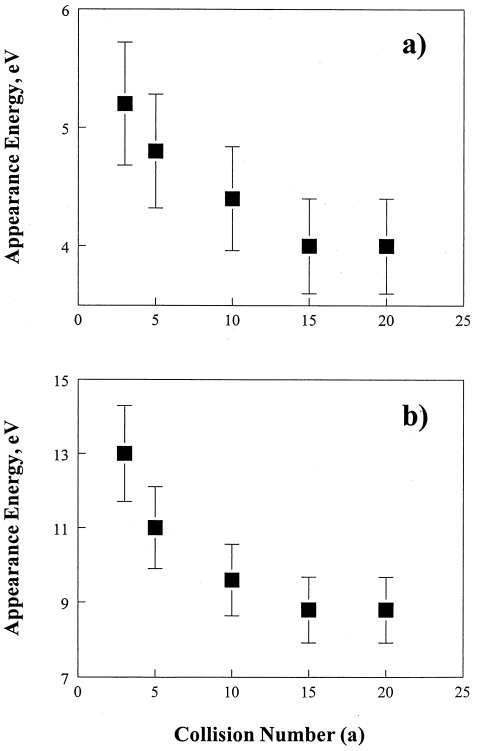

Fig. 9. Appearance energies as a function of Ar pressure in the cell for (a) *m/z* 51 and (b) *m/z* 50.

to note that the appearance energy for Reaction (R1) remains essentially constant with increasing Ar pressure (and the collision number) whereas the appearance energies of $C_4H_3^+$ and $C_4H_2^{+}$ formation decrease (see Fig. 9 and discussion in Sec. 3.6).

Fragmentation pathways of the bromobenzene radical cation observed in the present study are summarized in Scheme 1.

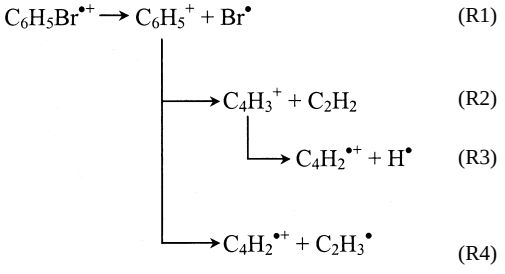

Scheme 1.

There is strong experimental evidence that $C_6H_5^+$ produced from bromobenzene has a cyclic, phenylium structure. Ion–molecule reactions of $C_6H_5^+$ produced from a number of precursors are characteristic of a cyclic phenylium structure [41]. CID and charge-stripping reactions of $C_6H_5^+$ revealed that a mixture of cyclic and acyclic isomers is produced by electron impact ionization formed from a variety of neutral precursors [42]. However, it has been shown that a major fraction of $C_6H_5^+$ ions formed from bromobenzene has the phenylium structure. Therefore we will further assume that $C_6H_5^+$ produced in Reaction (R1) is a phenyl cation.

3.3. Modeling of the fragmentation efficiency curves

Mass spectra may be calculated by knowing (1) the fragmentation reaction sequence of the ions, (2) the energy-dependent unimolecular rate constants of each

reaction, (3) the reaction time, and (4) the internal energy distribution of the fragmenting ions. In principle, if parameters 1–3 are known, the internal energy distribution may be extracted from the mass spectrum. This concept has been employed in the present study to develop a model that can determine CEDF from fragmentation efficiency curves.

The dissociation rate of internally excited ions may be calculated using the microcanonical RRKM/QET expression:

$$k(E) = \frac{\sigma W^{\ddagger}(E - E_0)}{h\rho(E)} \tag{8}$$

where $\rho(E)$ is the density of states of the reactant, $W^{\ddagger}(E - E_0)$ is the sum of states of the transition state, E_0 is the critical energy, h is Plank's constant, and σ is the reaction path degeneracy.

Fragmentation probability as a function of the internal energy of the parent ion and the experimental observation time (t_r), $F(E, t_r)$, is calculated based on the reaction scheme and the energetics of different reaction pathways. The function $F(E, t_r)$ is commonly referred to as a breakdown curve. A collection of breakdown curves, called the breakdown graph (BDG), is then constructed from the individual breakdown curves calculated for each reaction channel.

Collisional activation produces ions with a wide distribution of internal energies, $P(E, E_{CM})$. The contribution of ions having internal energy E to the observed signal intensity for a particular reaction channel i equals $F_i(E, t_r)\,P(E, E_{CM})$. Integrating over internal energies yields an overall signal intensity at a given CM energy, $I(E_{CM})$.

$$I(E_{CM}) = \int_0^{\infty} F(E, t_r)\,P(E, E_{CM})\,dE \tag{9}$$

Integration is performed from 0 to infinity because, in general, the ion can acquire rather high internal energy in multiple collisions with neutral molecules.

Modeling of the fragmentation efficiency curves presented in this study was performed as follows: (1) Dissociative rates were calculated using Eq. (8) for each reaction channel. (2) A breakdown graph was constructed from the individual breakdown curves, $F_i(E, t_r)$. (3) The energy deposition function was described by the following analytical expression:

$$P(E, E_{CM}) = E^l \exp[-E/f(E_{CM})]/C \tag{10}$$

where l is a parameter, $C = \Gamma(l + 1)[f(E_{CM})]^{l+1}$ is a normalization factor. Different forms of $f(E_{CM})$ will be examined in this article. (4) Relative signal intensities of different ions were calculated using Eq. (9) and compared with experiment.

3.4. RRKM/QET calculations

In the modeling presented here only Reactions (R1), (R2), and (R3) were considered. The rate-energy relation for Reaction (R1) has been extensively studied using different experimental [29,30,33,43,44] and theoretical methods [45–47]. RRKM calculations of the dissociation rate-energy curves for Reaction (R1) were carried out using vibrational frequencies of $C_6H_5Br^{+\cdot}$ obtained at the B3LYP level by Klippenstein [45]. The critical energy (E_0) of 2.76 eV proposed by Rosenstock and co-workers [33] was employed in the calculations. Transition state frequencies for Reaction (R1) were adopted from [44]. The entropy of activation ($\Delta S^{\ddagger}$) 8.07 e.u. was obtained using this set of frequencies (the same $\Delta S^{\ddagger}$ was used by Rosenstock et al. [33]). Because Reaction (R1) proceeds via a totally loose transition state it has been argued by Lim et al. [44] that simple RRKM modeling is not theoretically acceptable for this type of reaction. Nevertheless, these same authors agree that the RRKM model used here reproduces experimentally determined rate-energy dependence spanning over nearly six orders of magnitude for calculated rate constants.

Whereas energetics and dynamics of Reaction (R1) have been extensively studied and discussed, little information is available on Reactions (R2) and (R3). Jones et al. have measured the kinetic energy release for C_2H_2 loss from $C_6H_5^+$ from various precursors

[48]. The reported values, $T_{50\%}$, are lower than 40 meV, providing evidence that Reaction (R2) proceeds via a loose transition state. Similar results were obtained by Lifshitz et al. for Reaction (R3). A fairly narrow pseudo-Gaussian metastable peak for this reaction was observed [49]. Vibrational frequencies of the phenyl cation were adopted from [45]. The frequency (700 cm^{-1}) was taken as the reaction coordinate and the other five were set equal to 130 cm^{-1} leading to an activation entropy of 4.5 e.u. Energetics of Reactions (R2) and (R3) were estimated based on thermochemical data from [50]. Using these data one obtains ΔH_r (R2) = 76.2 kcal mol^{-1} (3.3 eV) and ΔH_r (R3) = 101.1 kcal mol^{-1} (4.38 eV). These values were used as initial guesses for critical energies for these two reactions and varied to give a best fit to the experimental fragmentation efficiency curves.

Because $C_4H_3^+$ is a relatively small ion it totally dissociates on the timescale of our experiment (5 s) as soon as an internal energy infinitesimally above the fragmentation threshold is deposited into the ion. Therefore Reaction (R3) was treated in the "sudden death" approximation—that is, it was assumed that its precursor ion is totally decomposed at any energy above the fragmentation threshold. This reaction is important only at CM energies above 10 eV. It follows that any deficiencies that arise from the use of this approximation will be apparent only at very high energies.

3.5. Results of theoretical modeling

The experimental fragmentation efficiency curves for $C_6H_5Br^{+\cdot}$, $C_6H_5^+$, and $C_4H_3^+$ were compared to the results obtained with this model (Figs. 10 and 11). It is clearly seen that the same theoretical model can reproduce the on-resonance single-collision and SORI experiments. The best agreement between experiment and theory was found for $f(E_{CM})$ [Eq. (10)] in the following form:

$$f(E_{CM}) = A_2E_{CM}^2 + A_1E_{CM} + E_{th}/(l + 1) \qquad (11)$$

where A_1 and A_2 are parameters, E_{th} is the average thermal energy at 298 K, and l is the same as in Eq. (10). The last term in Eq. (11) was added based on the following considerations. Average energy calculated over the distribution of internal energies in its general form [see Eq. (10)] is given by the following expression:

$$\langle E\rangle = (l + 1)\, f(E_{CM}) \qquad (12)$$

Using $f(E_{CM})$ from Eq. (11) in the limiting case when $E_{CM} \rightarrow 0$ one obtains $\langle E\rangle = E_{th}$. Thus, the last term in Eq. (11) is added to satisfy the initial conditions, i.e. in the collision free limit the ions have a nonzero thermal distribution of internal energies.

Parameters used to obtain the best fit shown in Fig. 10 are summarized in Table 2. An additional parameter, reactive fraction (r), was introduced to account for the percentage of the ion population that does not collide with Ar and therefore cannot participate in the fragmentation process. The reactive fraction that gave the best fit for the on-resonance single-collision experiment is 0.019. This value is in excellent agreement with the fraction of ions that undergo one collision ($Q_1 = 0.02$) under the conditions utilized in this experiment. The reactive fraction for SORI-CID experiments increases with collision number (~68% at $a = 3$ to almost 100% at $a = 15$); i.e. at higher pressures more ions participate in CID as a result of collisions with the neutral target.

The critical energy for Reaction (R2) that gave the best fit to our experimental results is 3.75 ± 0.15 eV. This value is 0.45 eV higher than E_0 calculated based on heats of formation of phenyl cation and $C_4H_3^+$. However, the heat of formation of $C_4H_3^+$ is not a firmly established value, as indicated in [50]. Interestingly, the critical energy for Reaction (R3), 3.95 ± 0.10 eV, obtained in this study, is 0.43 eV lower than the value estimated based on the available thermochemical information. Both (R2) and (R3) proceed via loose transition states (see discussion in Sec. 3.4). A loose transition state is indicative of a negligible reverse energy barrier. As a result, one can estimate the heat of formation of $C_4H_3^+$. Thus we conclude that the heat of formation of $C_4H_3^+$ is about 0.44 eV higher than the value listed in [50].

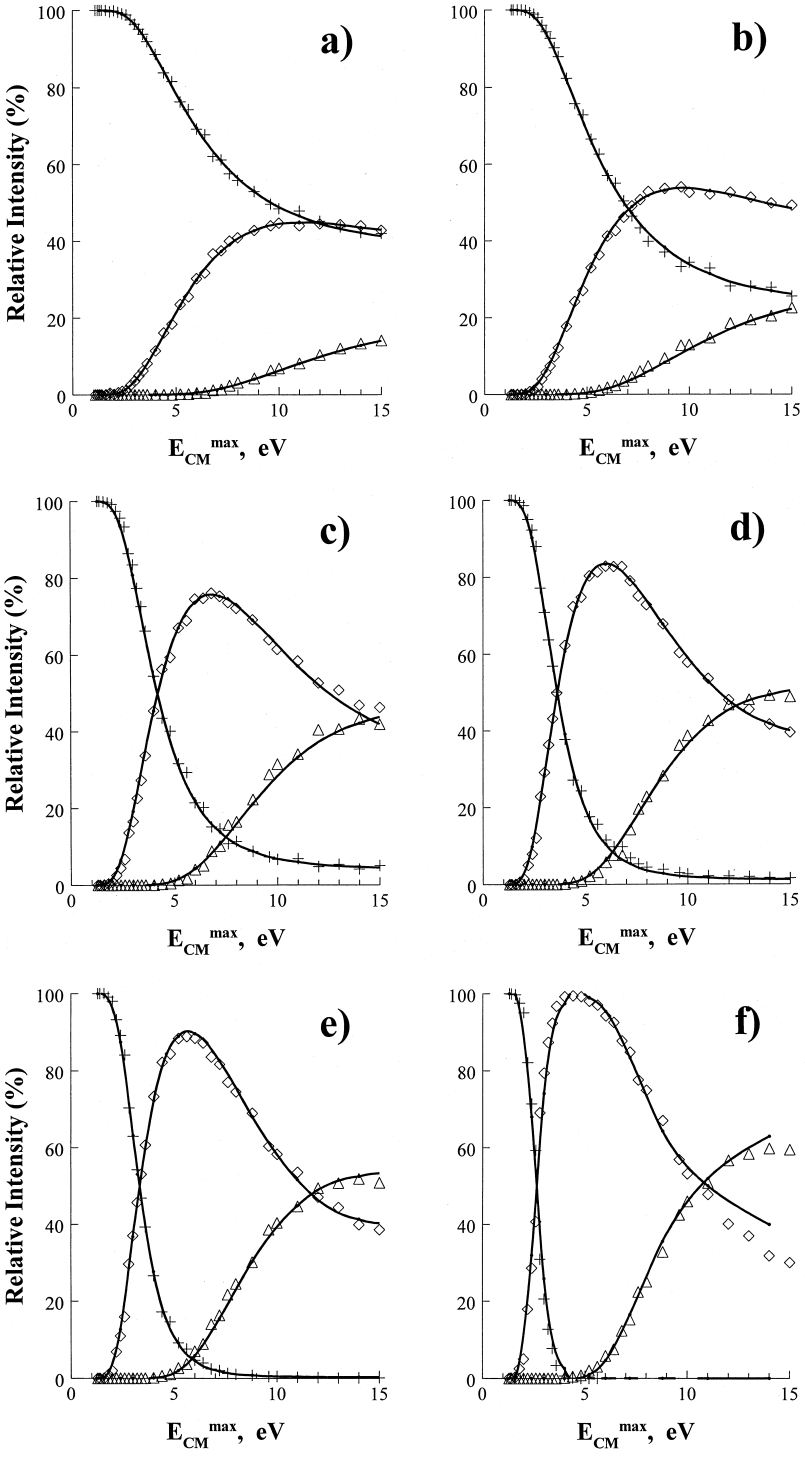

Fig. 10. SORI-CID fragmentation efficiency curves for (plus) *m/z* 156, (diamond) *m/z* 77, and (triangle) *m/z* 51 and results of theoretical modeling (solid line) for (a) $a = 3$; (b) $a = 5$; (c) $a = 10$; (d) $a = 15$; (e) $a = 20$; (f) $a = 100$.

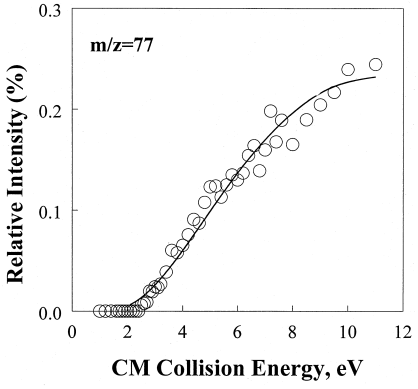

Fig. 11. Experimental curve (circles) and theoretical model (solid line) for the on-resonance experiment under single-collision conditions.

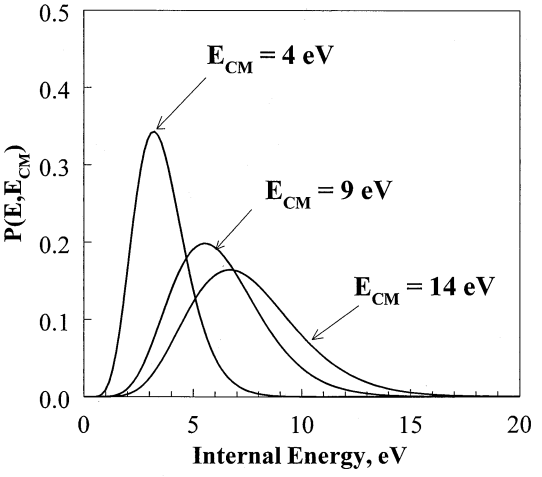

Fig. 12. Dependence of collisional energy deposition function on the center-of-mass energy for 10-collision experiment.

3.6. Collisional energy deposition function (CEDF)

The collisional energy deposition function that we deduce for multiple-collision experiments is a bell-shaped, Boltzmann-like function. The influence of several experimental parameters on the CEDF and the average energy transferred upon collisions can now be examined.

(1) The dependence of CEDF on the center-of-mass collision energy for $a = 10$ is illustrated in Fig. 12. At higher CM energies the distribution becomes wider and the maximum shifts to higher internal energies.

(2) The pressure dependence of the CEDF at 9 eV center-of-mass energy is presented in Fig. 13. For the on-resonance single-collision experiment the CEDF decreases exponentially with an increase in internal energy. This result is in line with our expectations, because exponential decline of the efficiency of energy transfer with increasing internal energy is characteristic for inefficient energy transfer ("weak colliders" model) [51].

For multiple-collision experiments, the maximum of the CEDF shifts toward higher internal energies as the pressure increases. However, the width of the distribution remains unchanged. The only exception is a 100-collision experiment, for which CEDF is significantly narrower. In order to test the reliability of the model used in this study, the same modeling was performed assuming that ions have a thermal distribution of energies. The same quality fit to the one shown in Fig. 10 could be obtained for the high-pressure experiments ($a = 15$, 20, and 100). However, the data from the lower pressure experiments

Table 2
Parameters used for modeling of the fragmentation efficiency curves

Collision number (a)	E_0(R2), eV	E_0(R3), eV	Reactive fraction (r)	A_1	A_2	l
0.02			0.019	0.234	−0.01056	0
3	3.85	4.00	0.68	0.107	−0.00264	4.2
5	3.57	3.94	0.83	0.110	−0.00288	4.5
10	3.77	3.92	0.97	0.091	−0.00240	7.8
15	3.73	3.94	0.99	0.079	−0.00246	10.5
20	3.89	3.94	1.0	0.066	−0.00220	13.9
100	4.0	3.8	1.0	0.03	−0.00129	38.0

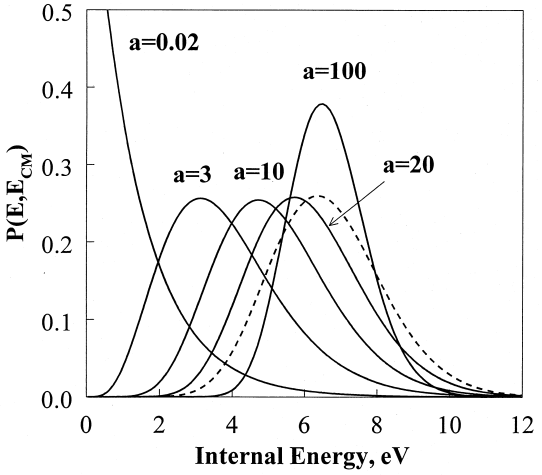

Fig. 13. Pressure dependence of collisional energy deposition function at 9 eV CM. Energy for the on-resonance experiment (a = 0.02) and SORI-CID experiments (a = 3, 10, 20, 100); dotted line shows a thermal distribution that gave a best fit to experimental data at this CM energy for a = 100.

(a = 3, 5, and 10) could not be reproduced using a thermal distribution. The thermal CEDF that gave the best fit for the 100-collision experiment at E_{CM} = 9 eV is shown in Fig. 13 (dashed line). The maximum of this distribution is found at about the same internal energy as that for the model function given by Eq. (10). However, the thermal CEDF is substantially wider. This observation suggests that modeling of high-pressure experiments is insensitive to the width of the energy distribution employed. Thus, the model function suggested in this study is preferable over the thermal CEDF because it is able to reproduce experimental results obtained over a wide range of pressures.

(3) The average energy transferred upon collisions is shown in Fig. 14 as a function of center-of-mass energy. The average energy rises nearly linearly at low collision energies and almost flattens at higher energies. Similar behavior of the average internal energy versus collision energy was observed by Lee et al. for collisional excitation of $CH_4^{+\cdot}$ [19] and by Wysocki et al. for $(C_2H_5)_4Si^{+\cdot}$ [20].

(4) Fig. 15 shows the dependence of the average energy transferred upon collisions on the number of collisions at several center-of-mass energies. At low

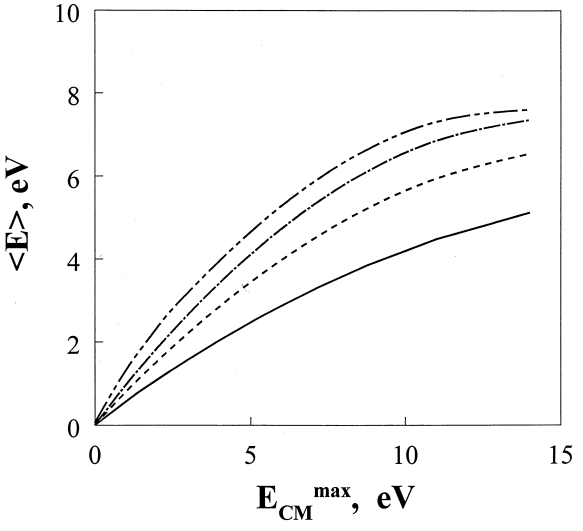

Fig. 14. Average internal energy transferred upon collisions as a function of the maximum center-of-mass energy of parent ion. E_{CM} = 1.5 eV (solid line); E_{CM} = 4 eV (dashed line); E_{CM} = 6 eV (long dash-short dash); E_{CM} = 9 eV (long dash-double short dash).

CM energies the average energy of the ion population shows a very weak dependence on pressure. However, for higher CM energies the dependence on pressure becomes more pronounced. This observation explains the fact that the appearance energy of the lowest

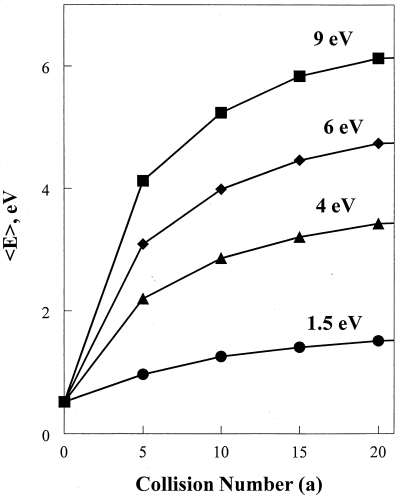

Fig. 15. Average internal energy transferred upon collisions vs. collision number (pressure) for different CM collision energies.

energy fragmentation pathway, leading to phenyl cation, was almost independent of pressure, whereas the appearance energies of *m/z* 51 and *m/z* 50, generated at much higher center-of-mass energies, exhibited a pronounced pressure dependence.

4. Conclusions

The present study provided a quantitative description of energy transfer upon SORI-CID excitation of the bromobenzene radical cation [52]. Knowledge of the energy deposition function is important both for understanding CID spectra resulting from "slow heating" and for extracting information on the energetics and dynamics of the observed fragmentation pathways.

Appearance energy for Reaction (R1) obtained using on-resonance excitation, 2.6 ± 0.2 eV at 298 K, is in good agreement with the values found in the literature. Our investigation of on-resonance CID lends further support that the use of this method of performing collisional activation of molecular ions in FTMS is equivalent in all respects to the analogous experiments carried out in sector instruments or using molecular beams. In particular, we demonstrated that threshold energies could be deduced with comparable accuracy to single beam studies of the same reaction. The smaller dynamic range of FTMS makes the experiments somewhat more tedious to execute than the corresponding sector-type experiment. The importance of very low conversions to ensure single collision conditions was reemphasized and the effect of multiple collisions to shift measured thresholds to lower values was demonstrated. These effects are also present in collision chamber experiments.

The effect of multiple collisions in increasing the efficiency of collisional activation in CID has been demonstrated qualitatively many times. Quantitative aspects were emphasized in the present article. For example, Table 2 demonstrates that the efficiency, denoted here as the fraction of ions that are reactive, rises sharply with increasing collision number. The reactive fraction was found to be equal to the collision number only for the single-collision on-resonance experiment, where the collision number was very low (0.02). However, the reaction efficiency approaches unity for an average collision number of 10 (corresponding to the average number of collisions equal to 6.3). Thus, at high pressures all of the ion population participates in the CID process. Unlike on-resonance CID experiments that require very low collision numbers for accurate threshold measurements, SORI-CID experiments are not restricted to single-collision conditions, and thereby are not limited by the dynamic range of the FTICR.

In this work an analytical expression for the collisional energy deposition function was proposed. Experimental results obtained over a wide range of experimental parameters, e.g. collision energies and pressures, were modeled using the same analytical form of the CEDF. An exponential energy deposition function gave the best fit to the single-collision experiment, whereas multiple-collision experiments were reproduced by a Boltzmann-like CEDF. Modeling fragmentation efficiency curves over a wide range of collision energies has the singular advantage that it is insensitive to experimental uncertainties.

A large amount of internal energy can be deposited into the ion upon SORI excitation. According to our results, threshold energy for the formation of $C_4H_2^+$ (*m/z* 50) is 10.5 eV. The high-energy fragmentation observed here is also found for other ions being investigated in our laboratories and elsewhere and is one of the key reasons the SORI technique is so useful in FTMS-CID. However, it is rather puzzling from fundamental considerations of the technique. It is generally believed that SORI-CID is effective in promoting only the lowest energy decomposition channels. Indeed, only parent ion motion can be stimulated by the off-resonance excitation. The irradiating field never excites fragment ions because their resonance frequencies are so far removed from the resonant frequency of the molecular ion. Further, the time between consecutive collisions is on the order of milliseconds. Because the unimolecular rate constant for the fragmentation of the bromobenzene radical cation rises sharply with internal energy, any molecular ion with internal energy content slightly above the fragmentation threshold will fragment before the

next collision will occur. According to this logic, there is no way to produce a highly vibrationally excited molecular ion using SORI excitation. However, high-energy fragmentation processes observed in this study indicate the opposite. This conclusion is inescapable because molecular energy transfer mechanism under the present experimental conditions is almost certainly from translational energy into vibrational energy of the ground state molecular ion.

We suggest the following possible rationalization of these observations. Although the fragment ions are not excited from the irradiating field, they do circulate in cyclotron orbits defined by their translational energy when they are formed by dissociation of the precursor ion. Ions with substantial translational energy undergo collisional activation leading to further dissociation. SORI excitation implies a broad distribution of translational energies, ranging from zero to the maximum value given by the appropriate equations. However, because the collision frequency depends on the kinetic energy of the ions, higher velocity collisions are selectively sampled. This effect becomes more pronounced as the amplitude of the irradiating field is increased. This facilitates the carry over of translational energy initially present in the dissociating parent ions into translation of daughter and granddaughter ions. These ions are subsequently collisionally activated and develop the sequence of reactions corresponding formally to very high internal excitation of the precursor ion. Thus our tentative conclusion is that SORI-FTMS-CID exhibits the same phenomenological characteristics as swarm or drift tube multiple-collision experiments in which collisional activation of not only the molecular parent ion but also subsequent generations of fragment ions occurs and contributes to the observed fragment ion spectrum. As a result, the collisional energy deposition function presented in this study should be considered as an "effective" CEDF, meaning that internal excitation leading to the unimolecular decomposition is due to collisional activation of the molecular ion and its subsequent fragments.

The heat of formation of $C_4H_3^+$ obtained from the modeling of fragmentation efficiency curves is 301 ± 4 kcal mole^{-1}. The ability to extract thermochemical information from SORI-CID measurements is surprising because the kinetic energy of the ions in SORI excitation is not well defined and the measured fragmentation patterns are an average over all the different collision energies attainable in the collisional activation process. However, in the modeling suggested in the present study we attributed the internal energy content of the molecular ion to the amount of fragmentation observed rather than to the initial kinetic energy of the molecular ion. This makes the present approach useful in extracting thermochemical information from the modeling of SORI-CID fragmentation efficiency curves.

Further experimental investigation of additional model systems is needed to determine the utility of the method presented in this investigation. It will be especially interesting to explore the applicability of the approach to the fragmentation of larger molecules, e.g. peptides.

Acknowledgements

This research was supported by NSF grants CHE-9616711 and CHE-9634238. We thank Professor D. P. Ridge and Professor C. Lifshitz for very helpful discussions.

References

[1] S.A. McLuckey, J. Am. Soc. Mass Spectrom. 3 (1992) 599.
[2] A.K. Shukla, J.H. Futrell, Mass Spectrom. Rev. 12 (1993) 211.
[3] R.N. Hayes, M.L. Gross, in J.A. McCloskey (Ed.), Methods in Enzymology, Vol. 193: Mass Spectrometry, Academic, Orlando, 1990, Chap. 10.
[4] E.M. Marzluff, J.L. Beauchamp, in T. Baer, C.Y. Ng, I. Powis (Eds.), Large Ions: Their Vaporization, Detection and Structural Analysis, Wiley, New York, 1996, Chap. 5.
[5] S.A. McLuckey, D.E. Goeringer, J. Mass Spectrom. 32 (1997) 461 and references therein.
[6] L.R. Thorne, J.L. Beauchamp, in M.T. Bowers (Ed.), Gas Phase Ion Chemistry, Vol. 3, Academic, New York, 1984, Chap. 18.
[7] R.E. March, R.J. Hughes, Quadrupole Storage Mass Spectrometry, Wiley, New York, 1989, p. 224.
[8] R.C. Dunbar, J. Chem. Phys. 95 (1991) 2537.

[9] R.C Dunbar, J. Phys. Chem. 98 (1994) 8705.
[10] W.D. Price, P.D. Schnier, E.R. Williams, Anal. Chem. 68 (1996) 859.
[11] W.D. Price, P.D. Schnier, R.A. Jockusch, E.F. Strittmatter, E.R. Williams, J. Am. Chem. Soc. 118 (1996) 10 640.
[12] R.C. Dunbar, T.B. McMahon, Science 279 (1998) 197.
[13] J.W. Gauthier, T.R. Trautman, D.B. Jacobson, Anal. Chim. Acta 246 (1991) 211.
[14] K.A. Boering, J. Rolfe, J.I. Brauman, Rapid Commun. Mass Spectrom. 6 (1992) 303.
[15] S.A. Lee, C.Q. Jiao, Y. Huang, B.S. Freiser, Rapid Commun. Mass Spectrom. 7 (1993) 819.
[16] A.J.R. Heck, L.J. de Koning, F. A. Pinkse, N.M.M. Nibbering, Rapid Commun. Mass Spectrom. 5 (1991) 406.
[17] R. Chawla, A. Shukla, J. Futrell, Int. J. Mass Spectrom. Ion Processes 165/166 (1997) 237.
[18] M.S. Kim, Int. J. Mass Spectrom. Ion Phys. 50 (1983) 189.
[19] S.H. Lee, M.S. Kim, J.H. Beynon, Int. J. Mass Spectrom. Ion Processes. 75 (1987) 83.
[20] V.H. Wysocki, H.I. Kenttämaa, R.G. Cooks, Int. J. Mass Spectrom. Ion Processes 75 (1987) 181.
[21] C.E.C.A. Hop, T.B. McMahon, G.D. Willett, Int. J. Mass Spectrom. Ion Processes 101 (1990) 191.
[22] A.R. Katritzky, C.H. Watson, Z. Dega-Szafran, J.R. Eyler, J. Am. Chem. Soc. 112 (1990) 2471.
[23] H.L. Sievers, H.-F. Grützmacher, P. Caravatti, Int. J. Mass Spectrom. Ion Processes 157/158 (1996) 233.
[24] M. Beyer, V.E. Bondybey, Rapid Commun. Mass Spectrom. 11 (1997) 1588.
[25] W. Zhong, University of Delaware, unpublished results.
[26] P.D. Schnier, J.C. Jurchen, E.R. Williams, J. Phys. Chem. B 103 (1999) 737.
[27] Because the ions are continuously accelerated/decelerated using this activation technique, the collision energy is not well defined but is oscillating with time. We refer here to the maximum collision energy attainable upon SORI-CID. This energy can be tuned to a desirable value by tuning the peak-to-peak voltage used in the excitation process.
[28] G. Bouchoux, Org. Mass Spectrom. 12 (1977) 681.
[29] S.T. Pratt, W.A. Chupka, Chem. Phys. 62 (1981) 153.
[30] Y. Malinovich, R. Arakawa, G. Haase, C. Lifshitz, J. Phys. Chem. 89 (1985) 2253.
[31] R.C. Dunbar, J.P. Honovich, Int. J. Mass Spectrom. Ion Processes 58 (1984) 25.
[32] T. Baer, B.P. Tsai, D. Smith, P.T. Murray, J. Chem. Phys. 64 (1976) 2460.
[33] H.M. Rosenstock, R. Stockbauer, A.C. Parr, J. Chem. Phys. 73 (1980) 773.
[34] D.J. Douglas, J. Phys. Chem. 86 (1982) 185.
[35] J.L. Beauchamp, Ann. Rev. Phys. Chem. 22 (1971) 527.
[36] D.P. Ridge, University of Delaware, private communication.
[37] P.B. Grosshans, A.G. Marshall, Int. J. Mass Spectrom. Ion Processes 100 (1990) 347.
[38] D. Smith, N.G. Adams, Phys. Rev. A 23 (1981) 2327.
[39] A.G. Marshall, F.R. Verdun, Fourier Transforms in NMR, Optical, and Mass Spectrometry: A User Handbook, Elsevier, Amsterdam, 1990, p. 239.
[40] S. Guan, G.-Z. Li, A.G. Marshall, Int. J. Mass Spectrom. Ion Processes 167/168 (1997) 185.
[41] C. Lifshitz, D. Gibson, K. Levsen, Int. J. Mass Spectrom Ion Phys. 35 (1980) 365.
[42] J.R. Eyler, J.E. Campana, Int. J. Mass Spectrom. Ion Processes 55 (1983) 171.
[43] T. Baer, R. Kury, Chem. Phys. Lett. 92 (1982) 659.
[44] S.-H. Lim, J.C. Choe, M.S. Kim, J. Phys. Chem. 102 (1998) 7375.
[45] S.J. Klippenstein, Int. J. Mass Spectrom. Ion Processes 167/168 (1997) 235.
[46] C. Lifshitz, F. Louage, V. Aviyente, K. Song, J. Phys. Chem. 95 (1991) 9298.
[47] J. Oh, K. Song, Bull. Korean Chem. Soc. 14 (1993) 404.
[48] E.G. Jones, L.E. Bauman, J.H. Beynon, R.G. Cooks, Org. Mass Spectrom. 7 (1973) 185.
[49] C. Lifshitz, D. Gibson, K. Levsen, I. Dotan, Int. J. Mass Spectrom Ion Phys. 40 (1981) 157.
[50] S.G. Lias, J.E. Bartmess, J.F. Liebman, J.L. Holmes, R.D. Levin, W.G. Mallard, J. Phys. Chem. Ref. Data 17 (Suppl. 1) (1988).
[51] R.D. Levine, R.B. Bernstein, Molecular Reaction Dynamics and Chemical Reactivity, Oxford University Press, New York, 1987, Chap. 6.
[52] Studying fragmentation of the bromobenzene radical cation was advantageous because it has very simple reaction kinetics in a wide range of internal energies.